Two-Frequency Radar Experiments for Sounding Glacier Ice and Mapping the Topography of the Glacier Bed

Kenneth C. Jezek, P. Gogineni, X. Wu, E. Rodriguez, Fernando Rodriguez-Morales, *Member, IEEE*, A. Hoch, Anthony Freeman, *Fellow, IEEE*, and John G. Sonntag

***Abstract*—We performed airborne experiments using 150- and 450-MHz radars to measure ice thickness on the Greenland ice sheet. Our objectives were to investigate to what degree surface clutter obscures the basal echo when airborne measurements are made at different elevations and at different frequencies. We also explored interferometric techniques for processing the data to form swath measurements of ice thickness. We found that surface clutter was minimal for either frequency when operated at low aircraft elevations (500 m above the ice sheet surface) or over benign regions of the ice sheet. Because signal-to-clutter ratios were favorable, we found that we could retrieve the swath measurements of ice thickness at both frequencies using an interferometric technique. At high elevation, surface clutter degraded the 150-MHz signal, but the nadir ice thickness was still retrievable. The basal return in high-elevation 450-MHz data was detectable only after additional beam-steering techniques were applied to the data to reduce the surface clutter signal. Results suggest that interferometric cross-track ice-thickness measurements can be successfully made given a sufficient number of antenna elements driven at either 150 or 450 MHz and flown at both high and low elevations over the interior ice sheet.**

***Index Terms*—Author, please supply your index terms/keywords for your paper. To download the IEEE taxonomy go to http://www/ieee.org/documents/2009Taxonomy_v101.pdf.** AQ1

I. Introduction

WE CONDUCTED airborne radar experiments during the fall of 2007 in Greenland to test concepts for sounding glacier ice and imaging the glacier bed topography [1]. Based on the results of preliminary experiments carried out in 2006, we sought to evaluate dual-frequency radar performance at 150 and 450 MHz over a variety of glacial regimes. We operated the radars as nadir sounding radars and synthetic aperture radar (SAR) cross-track interferometers. The experiments were designed to characterize surface and volume clutter across different glacial regimes (such as the dry northern interior ice sheet, the seasonally melted central and south ice sheet, and crevassed zones). Our long-range science goals are to perform high-spatial-resolution measurements of ice sheet thickness, basal topography, and physical properties of the glacier bed. Our technical goals are to provide information on future radar designs, in particular plans for implementing P-band radar systems operated from aircraft and possibly from spacecraft [2]–[4].

In this paper, we focus on measurements we made over the interior ice sheet in northwest and northeast Greenland. Our study areas are located in the dry-snow zone and the percolation zone. The dry-snow facies are characterized by the rare occurrence of surface melt. Consequently, structures in the upper parts of the firn are relatively simple and consist mostly of alternating layers of fine- to medium-grained firn. These are overlain by undulating snow drifts (sastrugi) at the surface that have a roughness of about 4–6 cm rms [5]. Near-surface structures in the percolation zone can include vertical ice pipes (approximately tens of centimeters long cylindrically shaped columns of refrozen surface melt entrapped in the firn) AQ3 and horizontal ice lenses (centimeters wide). We give examples of 150- and 450-MHz radar data collected at both high and low elevations above the surface of the ice sheet and demonstrate that surface clutter is a primary process in obscuring the basal echo at high elevations. We show that the surface clutter contribution can be reduced by application of beam-forming techniques. We go on to show that where basal echoes are strong, we can obtain strip mode interferograms from which it is possible to calculate cross-track ice thicknesses.

II. Radar Instrument

We developed radars for operation at 150 MHz with a bandwidth of 20 MHz and at 450 MHz with a bandwidth of 30 MHz with multiple receivers for sounding and imaging polar ice sheets [6]. The system, which was an outgrowth of the instrument used in our preliminary 2006 investigation [7], [8], consisted of six receivers used to collect and digitize signals from each element of an antenna array. The antennas consisted of two four-element dipole arrays mounted under each wing of the aircraft. One or more elements could be used to construct a transmit antenna array. We operated the radar both in sounder (multiple transmit elements) and ping-pong modes AQ4

Manuscript received May 14, 2010; revised July 6, 2010; accepted August 5, 2010. This work was supported in part by the NASA Earth Science and Technology Office and in part by the Office of Polar Programs of the National Science Foundation.

K. C. Jezek is with the Byrd Polar Research Center, The Ohio State University, Columbus, OH 43210-1002 USA.

P. Gogineni, F. Rodriguez-Morales, and A. Hoch are with the Center for Remote Sensing of Ice Sheets, The University of Kansas, Lawrence, KS 66045 USA.

X. Wu, E. Rodriguez, and A. Freeman are with the Jet Propulsion Laboratory, Pasadena, CA 91109 USA.

J. G. Sonntag is with URS Corporation, San Francisco, CA, and also with the NASA Wallops Flight Facility, Wallops Island, VA 23337 USA. AQ2

Digital Object Identifier 10.1109/TGRS.2010.2071387

TABLE I
RADAR SYSTEM SPECIFICATIONS

Radar Type	Interferometry
RF Carrier Frequency	150 MHz(Band I) 450 MHz(Band II)
RF Bandwidth	20 MHz(Band I) 30 MHz(Band II)
Transmit Pulse Duration	3 μsec and 10 μsec
Duty Cycle	10%
Receiver Dynamic Range	86 dB
Noise Figure	3.8 dB
Peak Transmit Power	800 W(Band I) 1600 W(Band II)
Sampling Frequency	120 MHz
Pulse Repetition Frequency(PRF)	10 kHz
Interferometric Baseline	20 m to 30 m
Number of Transmitters	1 (VHF/P-Band)
Number of Receiver Channels	6
Range Resolution	3 m to 7.5 m
A/D Dynamic Range	12-bit, 72 dB
Antenna	8 half-wave dipoles
Total Range	Up to 3 km

(alternating transmit elements) and collected data over several flight lines over the Greenland ice sheet. We also collected data over the smooth ocean surface to calibrate the system and determine antenna pattern. The system specifications are detailed in Table I.

A. RF Section and Digital System

The system operates sequentially at either 150 or 450 MHz. The radio-frequency (RF) section of the system is composed of a two-way high-power transmitter and up to eight independent receiver channels.

The transmitter generates a chirp signal of 3–10-μs duration using an arbitrary waveform generator (AWG) in combination with a frequency mixing stage. The latter upconverts the baseband signal generated by the AWG to higher frequencies centered at the carrier frequency of interest (either 150 or 450 MHz). The upconverted signal is then amplified by high-power amplifier modules. Two high-power pulsed amplifier modules were used for each frequency band. The peak output power for each module was up to 400 W (800 W combined) at 150 MHz and up to 800 W (1.6 kW combined) at 450 MHz. In order to minimize the harmonic distortion of the transmit signal, the amplifiers were operated in the linear power regime (below the 1-dB compression point) at both center frequencies. The instantaneous bandwidths of the system were 30 MHz during operation at 450 MHz and 20 MHz during operation at 150 MHz.

Each receiver channel has a maximum gain of about 72 dB and a measured noise figure of 3.3 dB or less (excluding antenna feed cable losses). The receivers are designed such that the gain can be adjusted over a 60-dB range in 1-dB steps. We incorporated absorptive RF (blanking) switches in the receiver chain for protection during the transmit event. A bank of switches and bandpass filters at the output of each receiver allows the user selection of the frequency band of operation. The band-limited output signal from each receiver is digitized with a 12-b analog-to-digital converter operating in undersampling mode at 120 MHz. The digitized data are stored on large-capacity Small Computer System Interface media controlled by a dedicated computer running a graphical user interface. The digitized data from each receiver channel are pulse compressed to provide real-time display of return as a function of range to check data quality during flight.

A common technique used to maximize the dynamic range of radio echo sounding instruments consists of recording data from two separate receiver channels, each with different gain settings, and then combining the data in postprocessing [9], [10]. In this system, the gain of each receiver is digitally controlled on a per-waveform basis. Low-receiver-gain settings (20–30 dB) are normally used to capture signal returns from the 3-μs pulses, while higher gain settings (60–70 dB) are used to amplify received echoes from the 10-μs pulses. Lower gain settings allow conditioning return signals with power levels as high as -16 dBm (operating in unsaturated mode), which come primarily from the ice surface as well as shallow internal layers. High-gain settings, on the other hand, allow detecting echoes from the ice/bedrock interface and deep internal layers. The minimum signal level that can be detected using high-gain settings is close to -149 dBm for both frequency bands (including signal processing gain). The resulting dynamic range for the instrument is on the order of 133 dB.

B. Antennas

We use half-wavelength dipole arrays as radiating structures. Each array is mounted below one wing of the aircraft. The array-element spacing is about 1 m, which is close to 1/2 λ at 150 MHz and 1.5 λ at 450 MHz, with λ being the free-space wavelength at the frequency under consideration. When used with multiple transmit antennas, the transmit array (left wing) uses an antenna feed network with Dolph–Chebyshev weighting designed to obtain low ($<$30 dB) sidelobes at 60°–80° incidence. The feed network is designed to accurately match the amplitude and phase balance between individual elements in the transmit array. The signals from each of the receive elements are digitized using separate channels. In the interferometric mode, we use the inboard elements of the antenna arrays for transmission on alternating pulses (ping-pong mode) and likewise digitize the received signals from the remaining elements. In sounder mode, the peak transmit powers are 800 W at 150 MHz and 1.6 kW at 450 MHz. For ping-pong operation, the peak transmit powers per side are 400 W at 150 MHz and 800 W at 450 MHz.

C. Data Collection and Radar Calibration

We collected data over the Greenland ice sheet, flying at altitudes as low as 500 m above the ice surface while terrain following and as high as 6.7 km above the ellipsoid. The system was operated in both interferometric and bistatic modes at 150 and 450 MHz. In ping-pong mode, we recorded four waveforms. We recorded a waveform from the left- and right-side transmit elements using a 3-μs pulse. We then recorded a second pair using a 10-μs pulse. Two pulses were used to

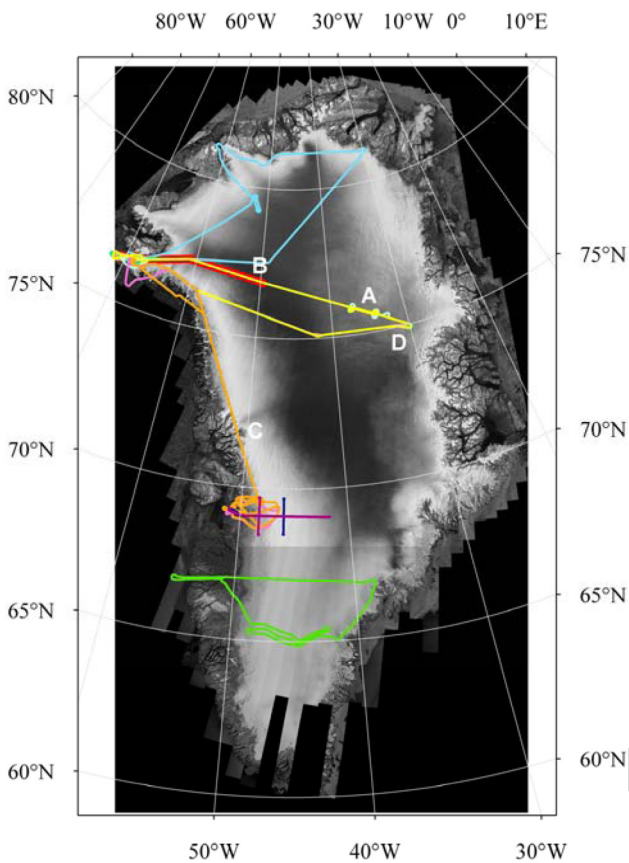

Fig. 1. Flights completed during September 2007 to test the GISMO concept. The yellow line in the upper third of the map intercepts the North East Ice Stream (A) on the eastern side, before turning back to cross study area D. It also follows the short path of a preliminary May 2006 experiment (thick red line) which includes study area B. The orange line crosses several outlet glaciers, including Rinks Glacier (study area C). The purple lines in southwestern Greenland indicate overflights of fast glacier regions, and the green lines indicate overflights of locations of multidecadal *in situ* study areas first established in 1980 by The Ohio State University.

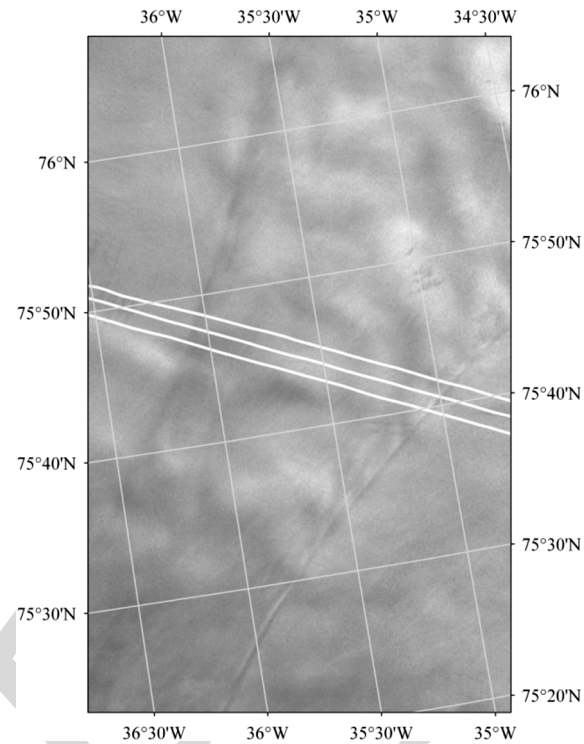

Fig. 2. Three closely spaced flight lines that are oriented orthogonally to the flow of the North East Ice Stream (location A in Fig. 1). The lines were reflown to within about 100 m at different frequency and aircraft elevation combinations. The ice stream appears as a funnel shape trending from lower left to upper right in this Radarsat-1 image.

increase the compressed power density at the base of the ice sheet and to reduce chances for near-surface returns to saturate the receivers. In bistatic mode, we used four transmit elements located on one wing and four receive elements located on the opposite wing. Only one frequency could be transmitted during a flight, and consequently, flight paths were repeated twice during most of these experiments. Antenna elements were manually lengthened or shortened prior to a flight to match the intended radar frequency. To calibrate the system and obtain the radiation pattern of the antenna arrays, we collected data over the smooth ocean surface [11]. This test also allowed us to validate the effectiveness of our predistortion technique for range sidelobe reduction. We also characterized the system using a synthetic target and a network analyzer. The synthetic target was built using a fiber-optic delay line to emulate the transmit signal propagation through 3 km of ice.

D. Aircraft Navigation and Attitude Control

Aircraft position and attitude information are computed post-flight by combining 2-Hz sampled global positioning system data and Litton 100 inertial navigation system data. Navigation and orientation data are provided by the NASA Wallops Flight Facility team who was on board each of our flights. Aircraft orientation accuracy is estimated at about $\sim 0.01°$. Geographic positional accuracy is estimated at 2 cm, and aircraft elevation is estimated to be about 10 cm. In addition, we verified roll accuracy over the ocean and over the flat interior ice sheet by comparing the phase of received signals across the receiver array wherein receiver-to-receiver phase biases were previously removed by internal calibration. This approach also provides additional control on phase noise due to wing flexure.

III. Greenland Field Experiments

Our 150- and 450-MHz experiments were conducted in September 2007 using the NASA P-3 aircraft equipped with GPS operated by the Wallops Flight Facility (Fig. 1). Flight lines are shown in Fig. 2. The most northerly 2007 flight line (thin blue line in Fig. 2) was designed to capture surface clutter conditions across outlet glaciers discharging into the Arctic Ocean and across the dry-snow zone. The second northerly leg (yellow in Fig. 2) again intercepted the dry-snow zone and passed over the NGRIP deep drilling site. The eastern portion of the flight repeatedly crossed the North East Ice Stream which is suspected of being underlain in parts by water [12]. As the experiment unfolded, we concentrated several flights over the North East Ice Stream as it provided good baseline data. We overflew this segment four times. We first operated at high altitude, at 450 MHz, and in ping-pong mode. We next operated at lower altitudes in bistatic mode (four transmitting

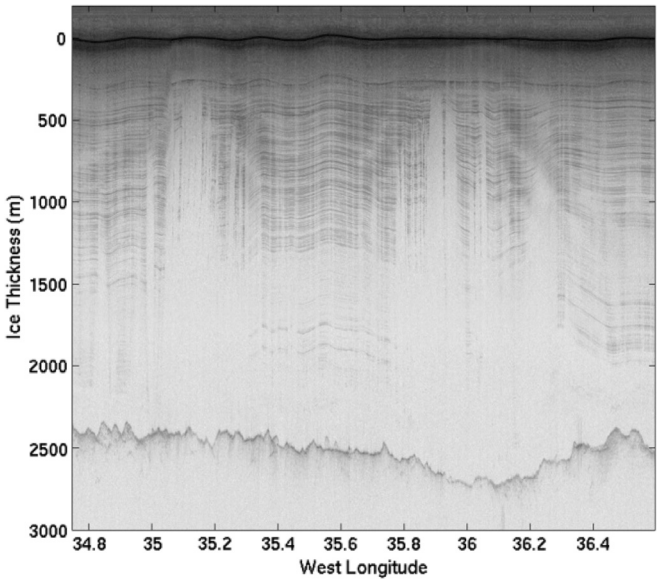

Fig. 3. Section of 150-MHz data across the North East Ice Stream. Sensor was operated in ping-pong mode and flown at 500 m above the ice sheet surface. Internal layers are distributed throughout the ice volume. The ice stream margins are located at approximately 35° and 36.1° W longitude.

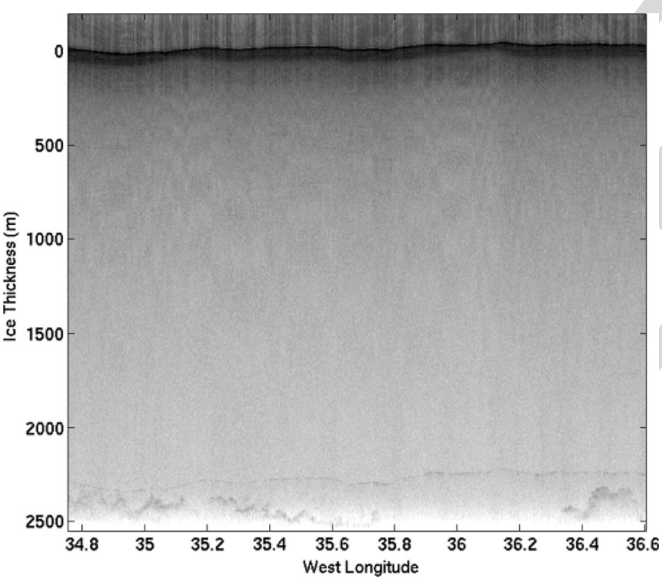

Fig. 4. Section of 150-MHz data across the North East Ice Stream. Sensor was flown in ping-pong mode about 4400 m above the ice sheet surface. The basal return appears in the later part of the record and exceeds the range window in the center right portion of the frame. Internal layers are undetected.

and four receiving antennas). We then operated at 150 MHz in ping-pong mode at high elevation. Finally, we flew the line outbound at 150 MHz in ping-pong mode and then configured the radar for the inbound leg in bistatic mode. The different combinations allowed us to look at clutter problems using different frequencies, different operating altitudes, and different transmit and receive configurations.

Additional lines were flown to collect data over other glacier regimes in central and southern Greenland where clutter issues are compounded by significant crevasses and/or substantial surface melt and refreezing of the upper firn layers. The long orange line in Fig. 2 parallels the ice margin intercepting several outlet glaciers, including Rinks Glacier, before continuing along and across the heavily fractured surface of Jacobshavn Glacier. The green line proceeds along several strain rate clusters installed by The Ohio State University in 1980.

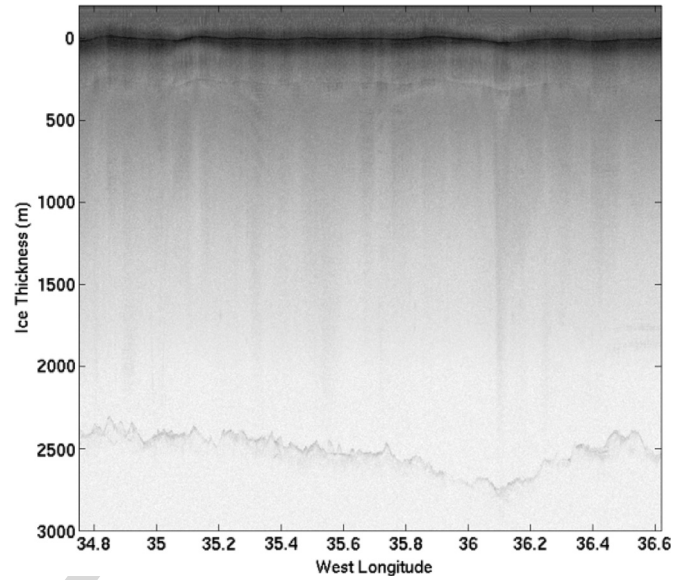

Fig. 5. Section of 450-MHz data across the North East Ice Stream. Sensor was operated in bistatic mode. Data from four transmitting elements and one receiving element are used here. The sensor flew at 500 m above the ice sheet surface.

IV. Signal Strength Observations

Here, we examine data collected along several closely spaced flight lines that are positioned orthogonal to the flow of the North East Ice Stream (Fig. 2). Ice sounding radar echoes were exceptionally strong in this region, presumably because the ice stream flows over a wet base. In this Radarsat-1 image, the ice stream appears as a more roughly textured band running from lower left to upper right. The center flight line intercepts the margins of the ice stream at 35° and 36.1° W longitude.

Figs. 3–6 show SAR-processed intensity-modulated displays of 150- and 450-MHz data collected along the center flight line. A presumming of 32 pulses is performed for each recorded waveform during data collection. The presummed data are then range and azimuth compressed, and the early part of the 3-μs records are combined with the later parts of the 10-μs records to yield seamless intensity images. In Figs. 3–5, the processed data from each of the six receiving channels are combined into a single record. At 500 m above the ice sheet surface, there is minimal surface clutter and a strong basal echo at 150 MHz (Fig. 3). Internal layers, which are associated with subtle changes in either the ice density or ice conductivity, are evident as are distortions in the intensity image at the margins of the ice stream. Fig. 4 shows the same section using the 150-MHz radar but flown at an altitude of 6700 m above the ellipsoid (about 4400 m above the ice sheet surface). The basal echo is located near the end of the range window. Notice the increase in surface clutter which is beginning to obscure the bottom echo. Here, internal layers are largely undetected. The

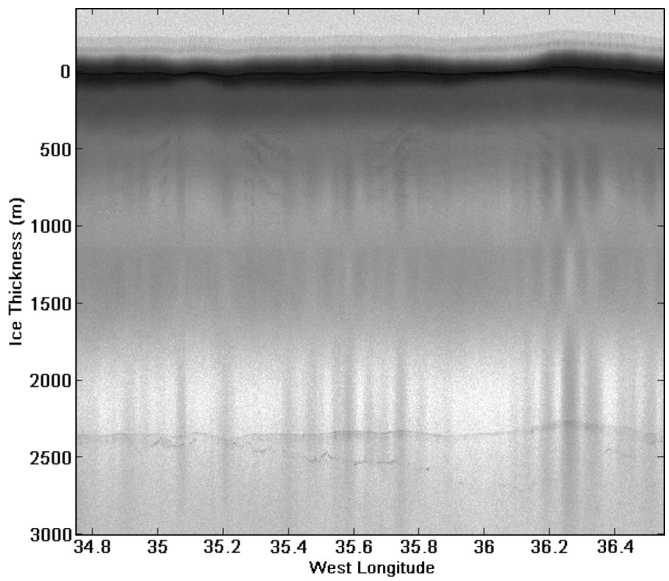

Fig. 6. Section of 450-MHz data collected at an altitude of about 4400 m above the ice sheet surface. The surface multiple spans the record at an equivalent ice thickness of about 2300–2400 m. The intermittent basal return appears at ice thicknesses between 2400 and 2700 m. The vertical stripping may be surface clutter (based on the somewhat similar appearance at different altitudes as shown in Figs. 5 and 6), or it may be related to uncompensated residual roll that would more strongly affect the 450-MHz data as compared to the 150-MHz data.

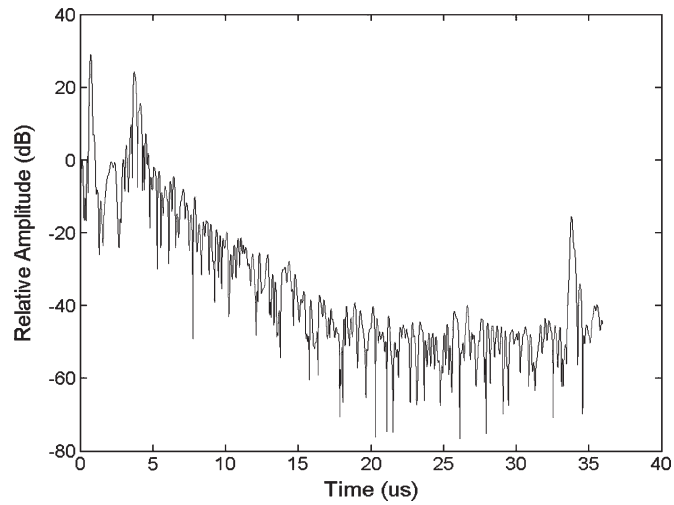

Fig. 7. 150-MHz amplitude display collected at an aircraft elevation of 500 m above the ice sheet surface. The basal return arrives at about 34 μs.

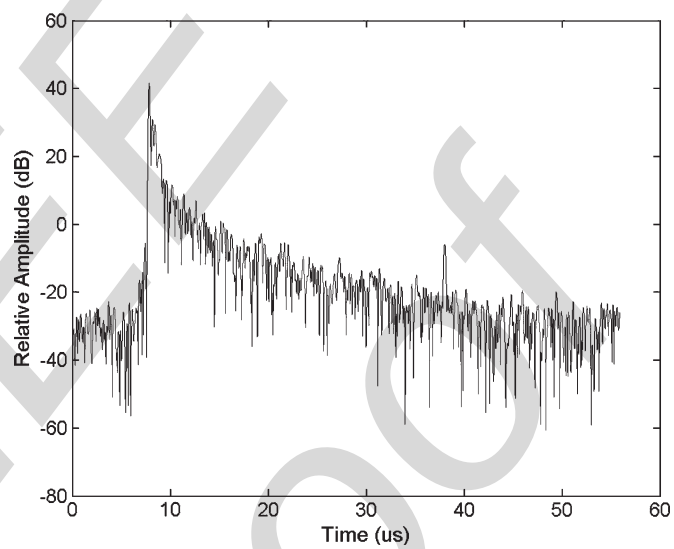

Fig. 8. 150-MHz echo amplitudes collected at an elevation of about 4400 m above the ice sheet surface.

fainter, generally horizontal line varying between about 2300 and 2400 m, is the surface multiple reflection.

Initial tests at 450 MHz revealed very low signal-to-clutter/noise levels in single-channel data sets. Therefore, we redesigned our experimental approach and flew the 450-MHz radar at 500-m elevation above the ice sheet with the system operated in a bistatic mode to increase the total power per waveform. We used four transmitting elements driven by two transmitters, and four receiving elements. The presummed data were SAR processed, and the receiving channels combined from which we were able to obtain a clear basal return (Fig. 5). We do not observe internal layers, but we do notice near-surface image patterns coincident with the eastern margin of the ice stream and similar to the patterns observed at 150 MHz.

We also collected data at 450 MHz in ping-pong mode at an altitude of 6770 m above the ellipsoid or about 4400 m above the ice sheet surface (Fig. 6). SAR processing the data and summing the channels alone did not retrieve the basal return from the surface clutter. We were able to reduce surface clutter by beam steering a combination of six phase centers positioned near the center line of the aircraft and formed from six receiving channels and the alternating transmit channels. We beam steered the three left and three right channels and did an incoherent sum with the beam-steered coherent result of the both sides. This substantially reduced the clutter and revealed the basal return along much, but not all, of the data segment. The surface multiple arrives at an equivalent ice thickness of 2400 m. The basal return is located just below the multiple and is intermittently observable above the surface clutter.

We quantitatively compared echo amplitudes by selecting measurements from nearly the same location and selecting the local maximum echo amplitude. We compared single-channel 150-MHz 3-μs-pulse low- and high-elevation range-compressed data. At low elevation (Fig. 7), the surface clutter is substantially reduced at time delays exceeding about 21 μs. The basal return is almost 20 dB above background noise. For the high-elevation observations (Fig. 8), surface clutter tapers smoothly along the record. The basal echo signal-to-clutter level at about 37 μs is about 10 dB. The waveform shape and the relative amplitude of the basal reflection to the local background suggest that, after accounting for additional spreading loss, there is about 8 dB of clutter adding to the high-elevation data at the arrival time of the basal echo.

We observed weaker signals relative to the background during low-elevation 450-MHz bistatic experiments even though we were transmitting more power per channel and used more transmitting channels in our bistatic configuration (Fig. 9). The tapered waveform in Fig. 9 suggests that surface clutter is largely absent past about 20-μs time delay at low elevation. We did not observe a basal return for similarly processed high-elevation 450-MHz data. We were only able to retrieve the basal

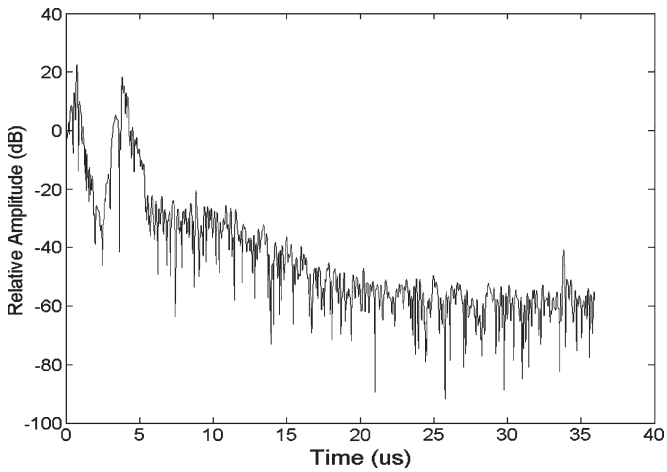

Fig. 9. Low-elevation 450-MHz waveform with bistatic antenna configuration.

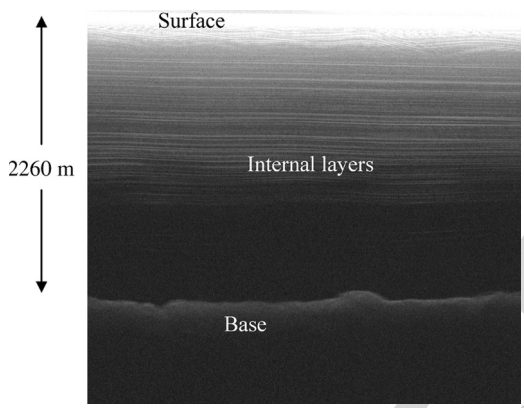

Fig. 10. 25-km-long 150-MHz SAR image collected over northwest Greenland (location B in Fig. 1).

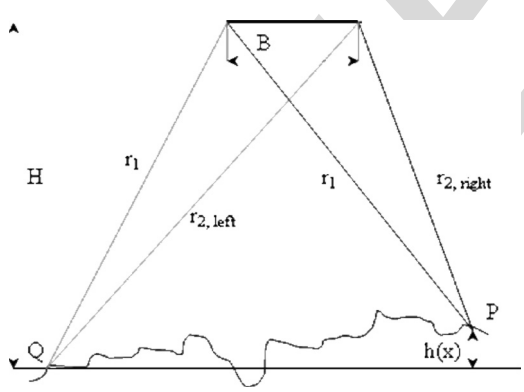

Fig. 11. Illustration of left–right signal contamination geometry.

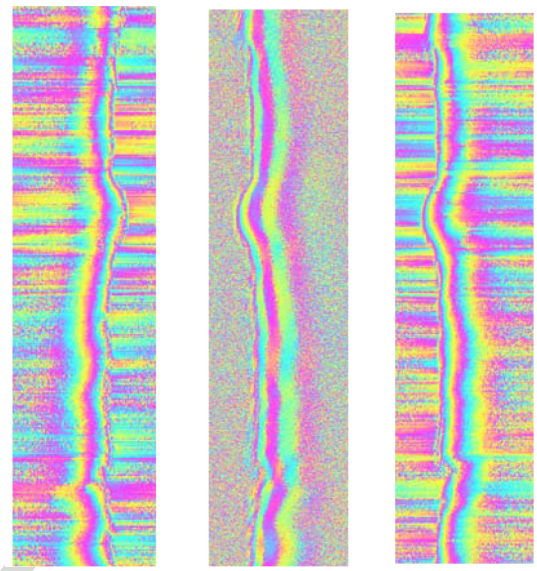

Fig. 12. (Center) Combined interferogram. Separated interferograms of signals from the left and right sides of the aircraft. Each record is 25 km long. The records are centered around the ranges corresponding to fringes from the glacier bed. The baseline is 3.91 m. 4/C

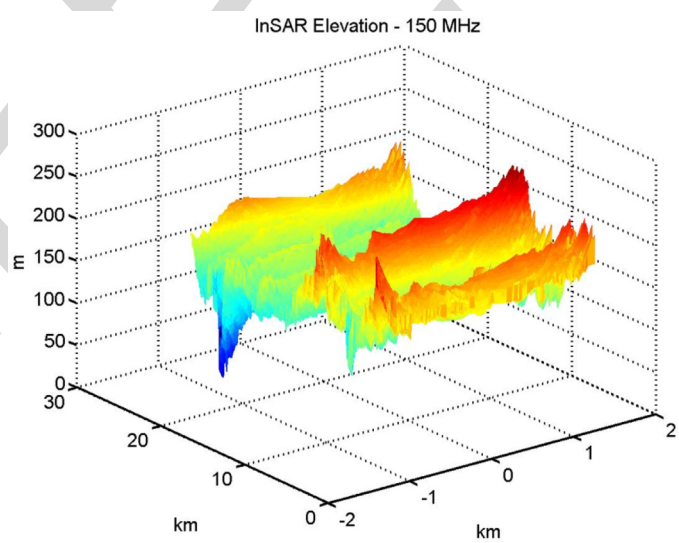

Fig. 13. Basal topography measured along a 25-km flight line and across a 3-km-wide swath over the western Greenland ice sheet in May 2006. The 150-MHz data were processed to simultaneously image the left and right sides of the aircraft. Note that the cross-swath dimension is exaggerated relative to the along-flight dimension (location B in Fig. 1). 4/C

return after application of beam-steering algorithms, which complicates amplitude comparison with the other examples.

The intensity display and amplitude data presented earlier suggest a strong elevation dependence on the signal-to-clutter levels at both frequencies. At low elevations, strongly attenuated arrivals from the base of the ice sheet are mixed with off-nadir arrivals from the surface (loss through the ice sheet is typically about 1–2-dB/m loss for these frequencies [13]). However, the corresponding incidence angle on the ice sheet surface is high (greater than 80° for our data), substantially reducing the scattering coefficient for the upper surface of the ice sheet. At high elevations, the corresponding surface incidence angle is reduced to about 57° for our geometry, thereby increasing the surface clutter contribution.

Consistency between our observations and the expected behavior of surface clutter supports our conclusion that surface clutter (or perhaps very near surface volume clutter) is a primary scattering process that confounds detecting the weak basal echo at high elevations. Our observations are also supported by a recent theoretical analysis by Niamsuwan [11] who implemented a low-frequency modification to the Brown model [14] for estimating high-frequency scattering from a rough

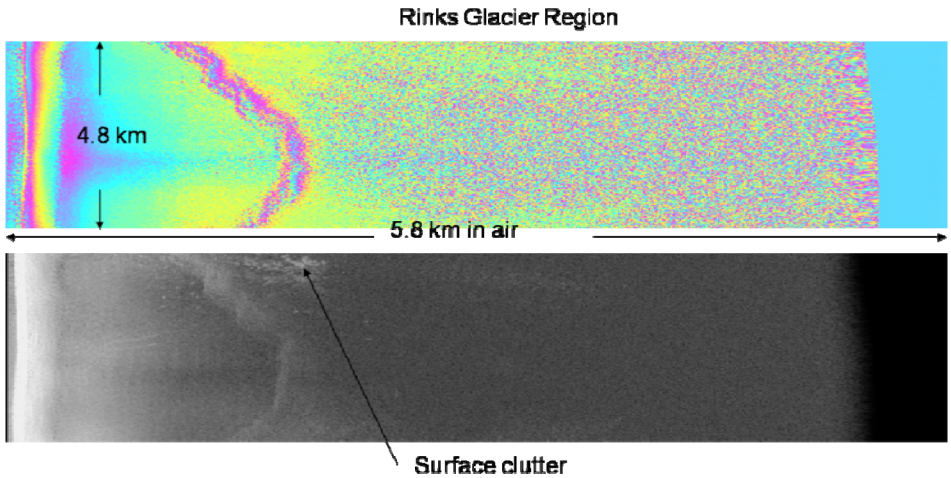

Fig. 14. (Upper) Interferogram phase image and (lower) SAR intensity image for a segment of 450-MHz data collected across Rinks Glacier in west Greenland (location C in Fig. 1). The thinnest ice is 500 m, and the thickest is 880 m in this scene. Off-nadir surface clutter is evident in the intensity image. The baseline for this geometry is 0.86 m. 4/C

surface. Using a physical optics model for the normalized radar cross section (NRCS), Niamsuwan applied the convolution approach to estimate the average pulse return waveforms from the upper and lower surfaces of the ice sheet. The analysis shows that, for a radar elevation of 500 m, a basal NRCS of -6 dB, 2-dB/m attenuation through the ice, and rms heights of the ice sheet surface between 1 and 5 cm, the basal return is separable from the surface clutter if the ice thickness is less than 2000 m for 150 MHz and 1800 m for 450 MHz (see [11, Fig. 5.7]). At 4-km elevation, the basal return is separable from the surface clutter only if the ice is less than 1300 m thick at 150 MHz and about 1100 m at 450 MHz. The maximum ice thickness increases if the attenuation through the ice sheet is decreased. For example, the basal and surface clutter returns are separable for ice thickness less than 2100 m for a 4000-m aircraft elevation if the attenuation is 1 dB/m. These predictions are quite close to our observations for basal return and clutter separation and further support the idea that surface/near-surface roughness properties are the primary clutter contributor. The significance of this conclusion is that the basal echo can be revealed by reducing surface clutter contributions using beam-steering techniques if sufficient numbers of receiving channels are available. This approach would not have been successful if volume scatter from within the interior of ice sheet were the primary clutter mechanism.

V. Interferometric Processing

We tested radar interferometric techniques as a method for reducing surface clutter and for constructing swath maps of subglacial topography. Using data from 2006 and 2007, we successfully processed multiple channels to form interferometric pairs similar to earlier surface-based experiments [15]. Fig. 10 shows an intensity image formed from 150-MHz data collected in 2006. Signals arriving after the strongest basal return are off-nadir arrivals and so represent intensity variations across the swath. Because of the isotropic radiation pattern of the dipole antennas, signals from the left and right sides of the aircraft are merged.

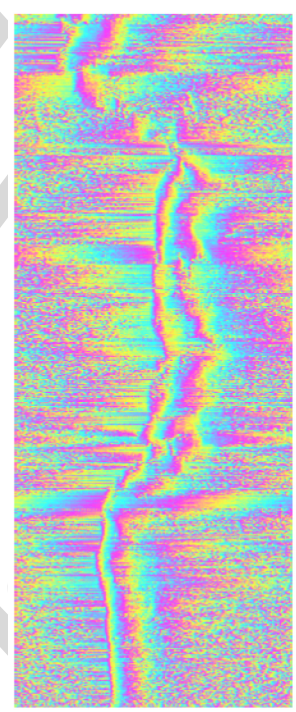

Fig. 15. Interferometric fringes for study area D in Fig. 1. The interferogram is 19 km long. The baseline is 86 cm. 4/C

Single-look complex images from two antennas were multiplied to form interferograms. Because each image is formed using a single dipole receiving antenna, the interferograms contain contributions from the left- and right-hand sides of the aircraft. We use the interferogram filtering scheme described in [2] and [16] to separate signals from the left and right side of the aircraft. We accomplish this by relying on the fringe rate properties across the interferogram. A single-layer geometry (Fig. 11) illustrates the essential elements of our problem. Here, B is the baseline separation between two phase centers, H is the height of the radar above some reference, $h(x)$ is the deviation of the actual surface from the reference, and P and Q are scattering points on the surface.

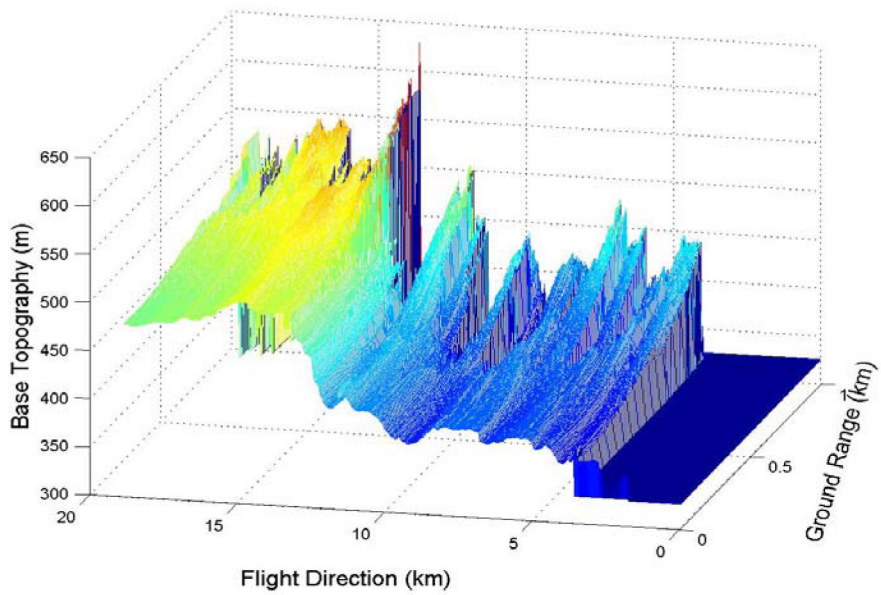

Fig. 16. Basal topography from 450-MHz interferometric data for location D in Fig. 1. 4/C

The range to the target point P from each of the two antennas is given by

$$r_1 = \sqrt{(H - h(x))^2 + \left(x + \frac{B}{2}\right)^2}$$

$$r_2 = \sqrt{(H - h(x))^2 + \left(x - \frac{B}{2}\right)^2}.$$

The range difference is

$$\Delta r = r_1 - r_2 \approx B\frac{x}{r_1}.$$

Forming the interferogram from each side of the array, we have

$$\begin{aligned} Int(r_1) &= S_1 S_2^* \\ &= A_1 A_2 \exp\{jk(r_1 - r_2\} \\ &= A_p \exp\left\{j\frac{4\pi}{\lambda}B\frac{x_p}{r_1}\right\} + A_q \exp\left\{j\frac{4\pi}{\lambda}B\frac{x_q}{r_1}\right\} \end{aligned}$$

where

$$x_p = \sqrt{r_1^2 - (H - h(x_q))^2} - \frac{B}{2}$$

$$x_q = -\sqrt{r_1^2 - (H - h(x_p))^2} - \frac{B}{2}.$$

The opposite signs of the exponentials in the interferogram mean that the fringe rates are different from the opposite sides of the aircraft. After including refraction (which may be a small correction depending on the aircraft elevation and swath width), the fringe rates allow for separation of the left/right signals via a simple bandpass filter.

The measured interferograms are shown in the center panel of Fig. 12 and include contributions from both the left and right sides of the aircraft. Signals from the left and right sides of the aircraft are obtained after bandpass filtering the measured interferograms and are shown by the left- and right-side panels in Fig. 12.

After unwrapping and correcting for refraction, the interferograms can be used to compute basal topography across, in the case shown, a swath of about 3 km wide (Fig. 13). Relative changes in ice thickness deduced from the interferograms are converted to an absolute ice thickness by using the direct nadir measurement and the computational methods outlined in [2] and [16]. Finally, the ice thickness is subtracted from a digital elevation model of the surface to construct the basal topography. Here, the northeast–southwest undulating topography has an amplitude of about 150 m.

We performed similar experiments at 450 MHz. As reported earlier, we found that signal strengths were substantially lower at 450 MHz even though we transmitted twice the power. This was partially compensated in regions of thinner ice. For example, we were able to create an interferogram from the low-elevation ping-pong mode data collected during the 2007 flight across Rinks Glacier (Fig. 14). The fringes were too sparse and too noisy to allow extraction of topography. Low fringe numbers pose a difficulty in measuring the fringe rate when trying to apply the interferogram filtering scheme. Baselines achievable on the P-3 aircraft limited the number of fringes.

We compensated for low signal strength in thicker ice by using four transmitting antennas to narrow and focus the beam. The results were successful, and we created SAR images of the base of the ice sheet of the North East Ice Stream. In this case, we were able to form interferograms that could be unwrapped (Fig. 15). Because we used multiple transmitting elements, the beam was already directional, and we did not need to separate the left and right signals. We did, of course, sacrifice half the potential swath width.

A 3-D depiction of the basal topography derived from the interferograms and a digital elevation model of the surface is shown in Fig. 16. Noise in the interferogram results in large data gaps across the topographic model.

VI. Summary

We have successfully retrieved ice-thickness measurements using 150- and 450-MHz airborne radar data collected over the Greenland ice sheet. We found that surface clutter is the primary scattering mechanism that obscures the basal echo as aircraft elevation is increased. As expected, the higher frequency 450-MHz data were more susceptible to clutter contamination than the lower 150-MHz data. We were able to overcome the high-elevation clutter problem at 450 MHz by applying beam-steering techniques that have previously been applied to 150-MHz data [8]. In cases where signal-to-clutter ratios were at least 10 dB, we were able to use interferometric techniques to estimate cross-track ice thicknesses and obtain strip maps of ice thickness along the flight track. We were able to increase the swath width of the strip by using a novel interferogram filtering technique to separate signals from the left and right sides of the aircraft.

References

[1] K. Jezek, P. Gogineni, X. Wu, E. Rodriguez, F. Rodriguez, J. Sonntag, A. Freeman, A. Hoch, and R. Forster, "Global ice sheet mapping orbiter concept: Airborne experiments," in *Proc. 7th Eur. Conf. Synthetic Aperture Radar*, 2008, vol. 2, pp. 99–102.

[2] K. Jezek, E. Rodríguez, P. Gogineni, A. Freeman, J. Curlander, X. Wu, J. Paden, and C. Allen, "Glaciers and ice sheets mapping orbiter concept," *J. Geophys. Res.*, vol. 111, no. E6, p. E06 S20, May 2006. DOI:10.1029/2005JE002572.

[3] K. Jezek, P. Gogineni, E. Rodriguez, X. Wu, J. Sonntag, F. Rodriguez, A. Freeman, and J. Curlander, "Global ice sheet mapping observatory—Final report," NASA ESTO, Greenbelt, MD, Dec. 2008, 57 p.

[4] K. Jezek, E. Rodriguez, P. Gogineni, A. Freeman, J. Curlander, X. Wu, C. Allen, W. Krabill, and J. Sonntag, "Glaciers and ice sheets mapping orbiter concept," in *Proc. 6th Annu. EUSAR*, Dresden, Germany, May 2006.

[5] C. J. Van der Veen, Y. Ahn, B. M. Csatho, E. Mosley-Thompson, and W. Krabill, "Surface roughness over the northern half of the Greenland Ice Sheet from airborne laser altimetry," *J. Geophys. Res.*, vol. 114, no. F1, p. F01 001, 2009. DOI:10.1029/2008JF001067.

[6] F. Rodriguez-Morales, P. Gogineni, C. Allen, C. Leuschen, K. Marathe, V. Jara-Olivares, A. Hoch, J. Li, J. Ledford, and K. Jezek, "Dual frequency and multi-receiver radars for sounding and imaging polar ice sheets," in *Proc. 7th Eur. Conf. Synthetic Aperture Radar*, Jun. 2008, vol. 2, pp. 95–98.

[7] C. Allen, S. Gogineni, B. Wohletz, K. Jezek, and T. Chuah, "Airborne radio echo sounding of outlet glaciers in Greenland," *Int. J. Remote Sens.*, vol. 18, no. 14, pp. 3103–3107, Sep. 1997.

[8] S. Gogineni, T. Chuah, C. Allen, K. Jezek, and R. K. Moore, "An improved coherent radar depth sounder," *J. Glaciol.*, vol. 44, no. 148, pp. 659–669, 1998.

[9] F. Hélière, C. Lin, H. Corr, and D. Vaughan, "Radio echo sounding of pine island glacier, West Antarctica: Aperture synthesis processing and analysis of feasibility from space," *IEEE Trans. Geosci. Remote Sens.*, vol. 45, no. 8, pp. 2573–2582, Aug. 2007.

[10] J. Dall, S. Kristensen, V. Krozer, C. Hernandez, J. Vidkjr, A. Kusk, J. Balling, N. Skou, S. S. Soebjaerg, and E. Christensen, "ESA'S POLarimetric Airborne Radar Ice Sounder (POLARIS): Design and first results," *IET Radar Sonar Navig.*, vol. 4, no. 3, pp. 488–496, Jun. 2010.

[11] N. Niamsuwan, "Electromagnetic scattering models for the global ice sheet mapping orbiter demonstrator," Ph.D. dissertation, Ohio State Univ., Columbus, OH, 2009, 148 p.

[12] M. Fahnestock, W. Abdalati, I. Joughin, J. Brozena, and P. Gogineni, "High geothermal heat flow, basal melt, and the origin of rapid ice flow in central Greenland," *Science*, vol. 294, no. 5550, pp. 2338–2342, Dec. 2001.

[13] J. Paden, C. Allen, S. Gogineni, K. Jezek, D. Dahl-Jensen, and L. Larsen, "Wideband measurements of ice sheet attenuation and basal scattering," *IEEE Geosci. Remote Sens. Lett.*, vol. 2, no. 2, pp. 164–168, Apr. 2005.

[14] G. S. Brown, "The average impulse response of a rough surface and its applications," *IEEE Trans. Antennas Propag.*, vol. AP-25, no. 1, pp. 67–74, Jan. 1977.

[15] S. Gogineni, D. Braaten, C. Allen, J. Paden, T. Akins, P. Kanagaratnam, K. Jezek, G. Presott, G. Jayaraman, V. Ramasami, C. Lewis, and D. Dunson, "Polar radar for ice sheet measurements (PRISM)," *Remote Sens. Environ.*, vol. 111, no. 2/3, pp. 204–211, Nov. 2007.

[16] Rodriguez, Principles of Interferometric Ice Sounding, in preparation. AQ6

Kenneth C. Jezek received the B.Sc. (Hons.) degree in physics from the University of Illinois, Urbana, in 1973 and the M.Sc. and Ph.D. degrees in geophysics from the University of Wisconsin–Madison in 1977 and 1980, respectively.

He is a former Director of the Byrd Polar Research Center, The Ohio State University, Columbus, where he is currently a Professor with the center and the School of Earth Sciences. His research interests include microwave remote sensing of the polar regions and have led several international campaigns to capture radar images of the Antarctic ice sheet from space.

P. Gogineni (F'XX) AQ7

He is currently a Deane Ackers Distinguished Professor with the Department of Electrical Engineering and Computer Science, The University of Kansas, Lawrence, and the Director of NSF Science and Technology Center for Remote Sensing of Ice Sheets (headquartered at The University of Kansas). He has been involved with radar sounding and imaging of ice sheets for more than 15 years and contributed to the first successful demonstration of SAR imaging of the ice bed through more than 3-km-thick ice.

Dr. Gogineni served as the Manager of the NASA polar program during 1997–1999. He received the Louise Byrd Graduate Educator Award at The University of Kansas and was a Fulbright Senior Scholar at the University of Tasmania, Hobart, Australia, in 2002.

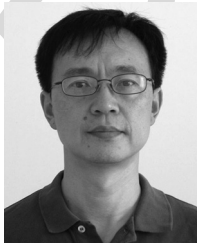

X. Wu received the B.S. and M.S. degrees in electrical engineering from Nanjing University of Aeronatics and Astronautics, Nanjing, China, in 1982 and 1985, respectively, and the Ph.D. degree from the University of Stuttgart, Stuttgart, Germany, in 1998.

He was involved in data system design and development for the Modified Antarctic Mapping Mission and contributed to producing the first Antarctic surface velocity map and the interferometric coherence map in the Jet Propulsion Laboratory, Pasadena, CA, where he has been involved in radar sounding and imaging since 2005 and has produced the first radar image of Greenland ice sheet bed. AQ8

E. Rodriguez, photograph and biography not available at the time of publication. AQ9

Fernando Rodriguez-Morales (S'00–M'07) received the B.S. degree in electronics engineering (*cum laude*) from the Universidad Autónoma Metropolitana, México City, México, in 1999 and the M.Sc. and Ph.D. degrees in electrical and computer engineering from the University of Massachusetts, Amherst, in 2003 and 2007, respectively.

From 2000 to 2001, he was with the Department of Physics and Astronomy, University of Massachusetts, where he collaborated in the development of single-electron transistor devices and semiconductor bolometer arrays. From 2001 to 2006, he was with the Department of Electrical and Computer Engineering, University of Massachusetts, developing ultrafast low-noise detectors based on superconducting devices, microwave monolithic integrated circuit amplifiers, and carbon nanotubes. Since 2007, he has been with the Center for Remote Sensing of Ice Sheets, headquartered at the Lawrence campus of The University of Kansas, where he supports and develops RF/microwave sensors and participates in field experiments in Greenland and Antarctica.

Dr. Rodriguez-Morales was the recipient of the Graduate Fellowship from the National Council for Science and Technology of Mexico.

A. Hoch, photograph and biography not available at the time of publication.

Anthony Freeman (M'83–SM'94–F'00) received the B.Sc. (Hons.) degree in mathematics and the Ph.D. degree in astrophysics from the University of Manchester Institute of Science and Technology, Manchester, U.K., in 1979 and 1982, respectively.

He is currently the Earth System Science Formulation Manager with the Jet Propulsion Laboratory (JPL), Pasadena, CA. JPL has a broad portfolio of Earth science missions as well as planetary science missions, and this office is responsible for all of JPL's future works in this area. Prior to this position, he was the Section Manager of the Mission and Systems Architecture Section at JPL, responsible for all advanced mission studies at JPL, and, prior to that instrument, Manager for the LightSAR Radar Program at JPL. He teaches a graduate-level class on "Remote Sensing Systems fromSpace" at the University of Southern California, Los Angeles. He is the holder of two patents. His research interests include correction of Faraday rotation, modeling of polarimetric radar scattering signatures, and the design of P-band spaceborne SARs.

Dr. Freeman has received the NASA Exceptional Service Medal for calibration of SIR-C mission data and numerous NASA new technology awards.

John G. Sonntag received the B.S. degree in aerospace engineering from Texas A&M University, College Station, in 1991 and the M.S. degree in aerospace engineering from the University of Texas, Austin, in 1993.

Since 1993, he has been with URS Corporation, San Francisco, CA. He is currently a Senior Scientist with the Airborne Topographic Mapper project team, NASA Wallops Flight Facility, Wallops Island, VA, and a Member of NASA's Operation IceBridge management team. He specializes in the application of precise GPS positioning technology to airborne remote sensing problems and in the applications of airborne lidar mapping to polar science.

AUTHOR QUERIES

AUTHOR PLEASE ANSWER ALL QUERIES

Please be aware that the authors are required to pay overlength page charges ($200 per page) if the paper is longer than 6 pages. If you cannot pay any or all these charges please let us know.

AQ1 = Please provide keywords.
AQ2 = The current affiliations of J. G. Sonntag were obtained from the vitae. Please check if correct and provide the postal code of URS Corporation.
AQ3 = '$\sim$ 10's of cm' was changed to 'approximately tens of centimeters'. Please check if correct.
AQ4 = All occurrences of 'Ping-Pong' were changed to 'ping-pong'. Please check if correct.
AQ5 = Fig. 1 was uncited in the body. Its citation was inserted here. Please check if correct.
AQ6 = Please provide the publication update and complete authors of Ref. [16].
AQ7 = Please provide educational background of 'P. Gogineni' and also the year when he started to become an IEEE fellow.
AQ8 = 'Jet Propulsion Laboratory, Pasadena, CA ' was inserted in this sentence to serve as the current affiliation of 'X. Wu'. Please check if correct.
AQ9 = Please provide photograph and biography of E. Rodriguez.
AQ10 = The acronym 'MMIC' was expanded as 'microwave monolithic integrated circuit'. Please check if correct.
AQ11 = Please provide photograph and biography of A. Hoch.
AQ12 = The sentences of the current affiliations of John G. Sonntag in the vitae were reworded for clarity. Please check if correct.

END OF ALL QUERIES